Mineralogy of Miocene phosphatic nodules in SE Sicily (Italy)

Giuseppe CULTRONE, Giorgio ANFUSO and Eduardo SEBASTIÁN

This paper describes the geochemistry and petrography of three phosphatic nodular deposits in Ragusa Province, south-east Sicily (Italy). Phosphate nodules of late Burdigalian age are dispersed in a soft, friable packstone matrix within the Irminio Member of the Ragusa Formation. Mineralogical analyses revealed large amounts of calcite (64 to 89 wt. %) and smaller quantities of carbonate-fluorapatite (CFA). P_2O_5 content was less than 18%. Microtextural observations demonstrated that phosphate precipitation occurred in the microenvironments in the sediment in confined spaces (i.e. cavities, perforations) and not in the shells of microorganisms. The crystals were all of a similar size (~1 mm), presented imperfections, and the $\{0001\}_{CFA}$ and the $\{10\overline{1}0\}_{CFA}$ forms were clearly apparent. These hexagonal prisms showed reduced growth along their c axis. Our data suggest that bacteria were involved in the precipitation of CFA.

Giuseppe Cultrone, Eduardo Sebastián, Department of Mineralogy and Petrology, University of Granada, Avda. Fuentenueva s/n, 18002 Granada, Spain, e-mail: cultrone@ugr.es; Giorgio Anfuso, Department of Geology, Faculty of Marine and Environmental Sciences, University of Cadiz, Polígono Río San Pedro s/n, 11510 Puerto Real, Spain (received: April 12, 2007; accepted: November 10, 2007).

INTRODUCTION

Geological interest in phosphatic sediments has been growing during recent decades because of their economic significance, especially in the fertilizer industry which consumes about 90% of world production (Zapata and Roy, 2004), and because they are useful in palaeoenvironmental and palaeooceanographic reconstructions (Carbone *et al*., 1987; Martín Algarra and Sánchez Navas, 2000; Chen *et al*., 2004).

Phosphatic deposits have been observed all around the world (Baturin, 1971, 2000; Reimers *et al*., 1990; Ilyin, 1997; Knight, 1999; Soudry, 2000) and have been recovered from the bottom sediments of oceans, e.g. off the coasts of South Africa (Birch, 1979), Peru and Chile (Froelich *et al*., 1988; Kim and Burnett, 1988), south-east India (Purnachandra Rao *et al*., 2000), southern California (Schuffert *et al*., 1994) and Florida (Fountain and McClellan, 2000). The largest phosphate deposits in Europe are the Upper Cretaceous phosphatic chalks that extend across parts of northern France, southern England and Belgium (Jarvis, 1992).

In palaeogeographical terms, autochthonous phosphatic sediments, associated with condensed neritic and pelagic deposits, are used to identify time-gaps in stratigraphic sequences (Marshall

and Ruffell, 2004). Their common mineral phase is francolite, a carbonate-fluorapatite (CFA), in which substitution for and structural distortion of the crystal lattice are usual (Matthews and Nathan, 1977; Sánchez Navas and Martín Algarra, 2001).

As for their genesis, Van Cappellen and Berner (1991) and Gunnars *et al*. (2004) stated that phosphatic particles can be produced by inorganic precipitation in seawater solutions, by high rates of organic matter degradation and, probably, by the dissolution of fish debris (Schenau *et al*., 2000; Soudry and Nathan, 2000). Furthermore, bacteria may induce the precipitation of a phosphorus-enriched organic gel and act as a precursor to an amorphous calcium phosphate which in turn evolves into francolite (Soudry, 1993; Krajewski *et al*., 1994; Martín Algarra and Sánchez Návas, 1995; Schwennicke *et al*., 2000). Lucas and Prévôt (1984) observed how the type of water involved (natural freshwater and seawater) influence the crystallinity of apatite synthesis by bacterial activity. Phosphate authigenesis represents an important oceanic sink for reactive phosphorus (Kim *et al*., 1999). The hypotheses that have been suggested for the formation of marine phosphorites are not necessarily exclusive, but they probably represent different stages of the same phosphogenic process (Jarvis, 1992).

This paper aims to provide new information about the phosphatic deposits in south-east Sicily (Italy), especially with re-

gard to their petrography and genesis, by analysing the characteristics of three outcrops in the province of Ragusa. Initial research on these phosphate nodules and their lithostratigraphic characteristics was carried out by Ragusa (1902), De Stefani (1912) and Cortese (1929). Later, a distribution map was obtained by Bommarito and La Rosa (1962) and confirmed by Tedesco (1966) who estimated that the phosphatic occurrences were of Aquitanian-Langhian age. Di Grande *et al*. (1978) stated that the phosphatic nodules appeared in discontinuous lenses, with the phosphatic cement being made up of francolite, which replaced an earlier carbonate. Further studies on such topics were carried out by Pedley and Bennett (1985) and Carbone *et al*. (1987) who found a great similarity between Sicilian and Maltese phosphorites.

GEOLOGICAL SETTING

The Hyblean Plateau (south-east Sicily, Italy) consists of a thick, non-deformed platform of Triassic to Quaternary calcareous rocks (Grasso, 1997). The phosphatic nodules of the Hyblean Plateau are contained within the bedded packstones at the base of the Irminio Member of the Ragusa Formation, which is made up of an alternating succession of marly limestones, coarse grained carbonate packstones and micro-grainstones

spanning Late Oligocene–Middle Miocene range. According to Carbone *et al*. (1987), autochthonous phosphatic nodules belong to the same depositional environment, which is characterised by the progressive transition from carbonate sedimentation to new erosive hardground conditions.

PHOSPHATIC NODULE OUTCROPS

We analysed the characteristics of three outcrops observed at the coastal area on the Biddemi River, the Irminio River and at an active cliff at Donnalucata (Fig. 1). The area of investigation is characterized by a flat topography because of fluvial and marine terraces. The most important outcrops belong to:

— the aforementioned Irminio Member (Lower–Middle Miocene Age), characterized by non-deformed, horizontal strata;

— fluvial/marine deposits, at the mouth of the Irminio River (Quaternary Age);

— marls of the Tellaro Formation (Middle Miocene Age);

— slope continental deposits, including blocks of different sizes within a silt matrix;

— quaternary grainstones rich in shell fragments, developed above all on tops of most important hills.

The three phosphorite outcrops are autochthonous (Carbone *et al*., 1987) and are located (Fig. 1): (1) close to the mouth of the Biddemi River, at the top of a 5 m high cliff lying
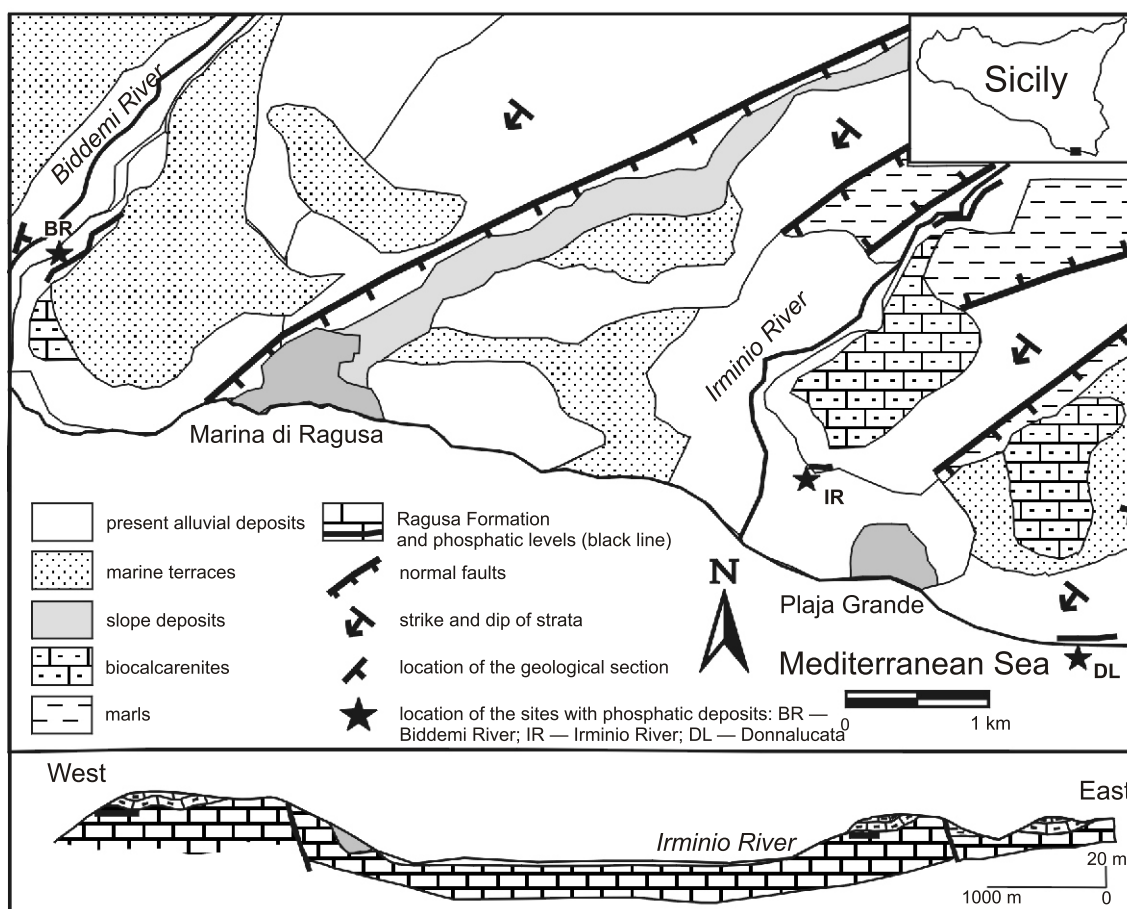

Fig. 1. Geological map and cross-section of Marina di Ragusa and surrounding areas (south-east Sicily)

directly on top of a crossed stratification; (2) at the mouth of the Irminio River, on a section cut by a coastal road; (3) on the cliff located between Plaja Grande and Donnalucata village. The three outcrops have similar features (Fig. 2): phosphate nodules are dispersed in a soft, friable, light-coloured packstone matrix in very distinct layers about 20 cm thick. Their brown colour creates a strong contrast with the yellowish, cream colour of the immediately underlying calcareous strata. Weathered surfaces are darker brown and have a rough texture. Nodules are well cemented and the most common shapes are subrounded and elongated. Their major axis ranges approximately from 2 to 10 cm and their minor one from 2 to 5 cm. The core area of the phosphatic nodules is quite uniform and dense with a distinctive, unvarying brown colour.

diffractometer with graphite monocromator, automatic slit and Cu$K\alpha$ radiation (λ = 1.5405 Å). The data were collected in step-scanning mode with 0.02° goniometer rate and 2θ from 3 to 60°. PXRD goniometric calibration was performed using a silicon standard. Phosphorite nodules were well-ground in a wolfram disk mill to <10 μm particle size and then analysed. The razor tamped surface (RTS) method (Zhang *et al*., 2003) was used to attain random particles orientation. The resulting data was interpreted using *XPowder* software (Martín, 2004). We performed a quantitative analysis of mineral phases converting the data to the constant sample volume and using the PDF2 data base and Normalized RIR method. No internal standard was added to the powder samples. *XPowder* software was used to make quantitative stud-
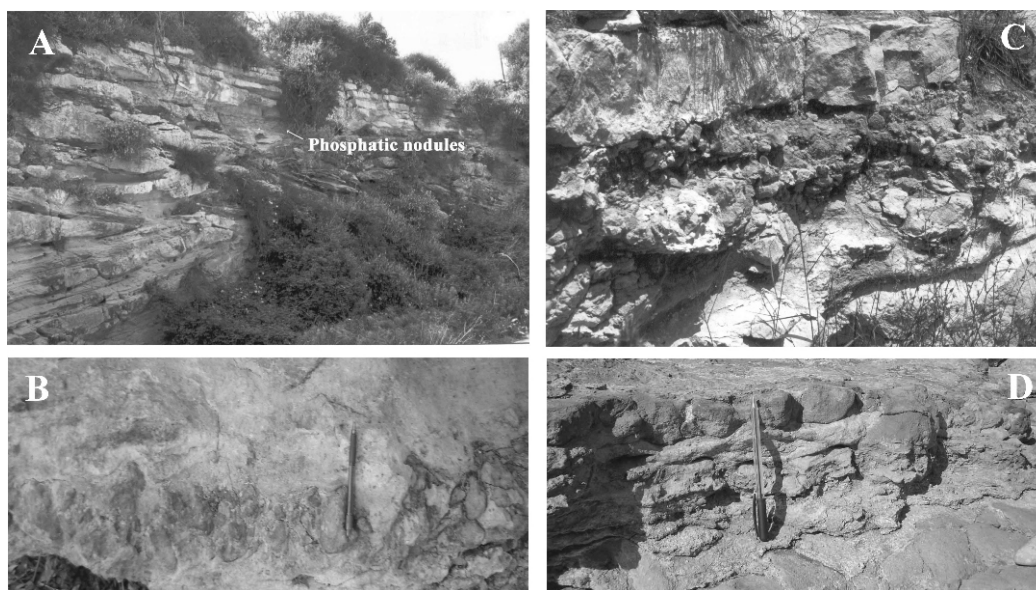

Fig. 2. Photographs of the studied outcrops

A — Biddemi River, phosphatic nodules lie on a cross stratified limestone; **B** — detail of the outcrop in A; **C** — 25 cm thick phosphatic layer at Irminio River; **D** — outcrop on the cliff between Plaja Grande and Donnalucata

ANALYTICAL METHODS

Texture, mineralogical and chemical composition of phosphorite nodules from Biddemi River (labelled as BR), Irminio River (IR) and Donnalucata (DL) were characterized. Analyses were carried out in the fresh brown cores of nodules in order to avoid alteration phases that could modify the mineralogy and chemistry of the phosphates. Bulk chemical analyses of nodules were performed by means of X-ray fluorescence (XRF; *Philips PW-1480*). 1 g per sample was finely ground and well mixed in agate mortar before being compressed into an Al holder for compressed XRF disk preparation. ZAF correction was performed systematically (Scott and Love, 1983). International standards (Govindaraju, 1989) were followed throughout. The estimated detection limit for major elements was 0.01 wt. %.

The mineralogy of the raw material was studied by powder X-ray diffraction (PXRD) using a *Philips PW-1710*

ies using methods of non-linear squared minimums on the full-profile fitting of the diffractograms making use of all the information in the PDF2 data base. Weighting was calculated using the Normalized RIR Method described by Chung (1974). RIR coefficients were obtained from the PDF2 database. The lattice parameters of CFA were refined because the length of the *a* axis varies depending on the carbonate content in crystals (LeGeros, 1965).

To characterize the texture and the microstructure of the nodules optical light microscopy (OLM; *Olympus BX-60*) and field emission scanning electron microscopy (FESEM; *Leo Gemini, 1530*) were employed. Two thin sections per sample type were prepared, one of which was polished. FESEM secondary electron (SE) and back-scattered electron (BSE) images were obtained using small sample pieces ($5 \times 5 \times 3$ mm in size) or polished carbon-coated thin sections. We also obtained Ca, P and F X-ray energy maps with the use of *EDX Oxford INCA-200* microanalysis.

RESULTS

X-RAY FLUORESCENCE

The results of this analysis indicate the high CaO content in all the samples (from 50.15% in DL3 to 55.23% in IR1). The P_2O_5 content was higher in the BR samples than in the other two groups of samples (Table 1). The SiO_2 content is very low and only slightly exceeds 2% in BR1, BR2, BR3 and DL3 samples. According to Slansky (1979), studied samples can be classified as phosphatic limestones nodules (P_2O_5 content is lower than 18%).

POWDER X-RAY DIFFRACTION

Diffractometric analyses show significant amounts of calcite and smaller amounts of CFA (Fig. 3). CFA values range from 10 to 36 wt. % (Table 2) and the highest CFA content appears in BR samples. Carbone *et al.*, (1987) indicated that the

Table 1

Concentration of major elements (wt. %) of phosphorite nodules

Sample	SiO_2	Al_2O_3	Fe_2O_3	MnO	MgO	CaO	Na_2O	K_2O	TiO_2	P_2O_5	LOI
BR1	2.03	0.65	1.07	0.01	0.66	51.41	0.34	0.24	0.02	16.21	26.24
BR2	2.37	0.57	0.97	0.01	1.00	52.51	0.96	0.16	0.08	15.38	25.97
BR3	2.35	0.60	0.96	0.01	1.03	51.70	0.93	0.14	0.19	16.75	25.31
BR4	1.47	0.32	0.65	0.01	0.85	51.12	0.88	0.12	0.10	13.60	30.90
IR1	0.17	0.22	0.35	0.01	0.47	55.23	0.04	0.09	0.01	7.96	35.76
IR2	1.43	0.31	0.66	0.01	0.85	51.58	0.84	0.12	0.07	13.40	30.75
IR3	1.05	0.25	0.37	0.01	0.74	52.92	0.57	0.07	0.09	10.24	33.69
IR4	1.93	0.45	0.81	0.01	0.86	50.91	0.74	0.15	0.09	12.87	31.16
IR5	1.25	0.35	0.36	0.01	0.77	53.19	0.45	0.06	0.06	7.65	35.85
DL1	0.49	0.34	0.41	0.02	0.73	53.37	0.75	0.13	0.00	4.37	39.85
DL2	0.84	0.26	0.28	0.02	0.93	53.56	0.46	0.06	0.03	3.02	40.49
DL3	2.12	0.50	1.25	0.02	1.10	50.15	1.04	0.18	0.04	4.62	38.97
DL4	1.20	0.36	0.37	0.02	0.99	51.18	1.13	0.08	0.07	4.73	39.89

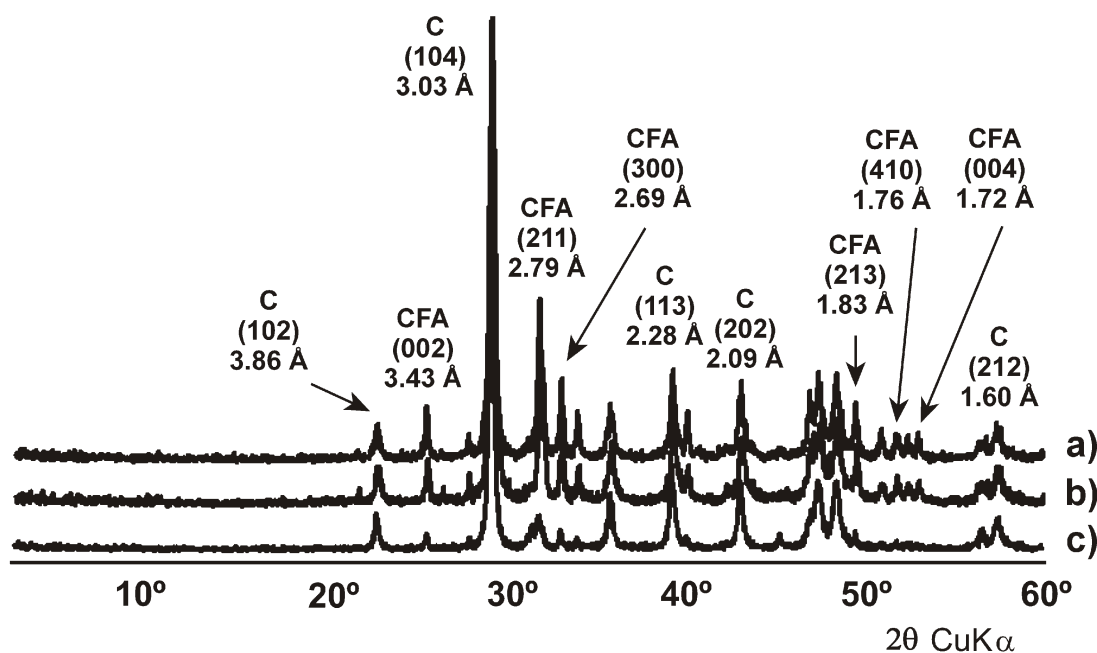BR — Biddemi River; IR — Irminio River; DL — Donnalucata

Fig. 3. PXRD diffractograms of Irminio River (a), Biddemi River (b) and Donnalucata (c) phosphatic nodules

C — calcite; CFA — carbonate-fluorapatite; CuKα X-ray radiation, λ = 1.5405 Å; main *hkl* Bragg peaks and d_{hkl} values are included

T a b l e 2

PXRD quantitative analysis (wt. %) of the three phosphorite groups

Sample	C		CFA		2	CO_3^{2-}(1)	CO_3^{2-}(2)
BR1	67.4	5.8	32.6	3.8	1.218	6.68	8.82
BR2	67.9	3.9	32.1	4.7	1.193	7.05	9.49
BR3	64.3	4.4	35.7	5.8	1.186	7.16	9.68
BR4	70.0	5.1	30.0	4.2	1.205	6.88	9.16
IR1	72.6	5.0	27.4	4.6	1.247	6.27	8.05
IR2	70.2	5.4	29.8	4.3	1.185	7.17	9.70
IR3	71.5	4.9	28.5	5.0	1.158	7.57	10.45
IR4	70.7	4.6	29.3	4.4	1.249	6.23	8.00
IR5	72.8	4.2	27.2	5.2	1.194	7.04	9.46
DL1	84.2	3.6	15.8	6.0	1.251	6.20	7.95
DL2	89.6	2.8	10.4	5.4	1.164	7.48	10.28
DL3	83.9	5.1	16.1	4.8	1.192	7.07	9.51
DL4	83.3	5.3	16.7	4.1	1.223	6.61	8.68

XRD 2 (004)–(410) and wt. % using Gulbrandsen (1) and Schuffert *et al*. (2) equations are also reported; other explanations as in Table 1 and Figure 3

darker colour of the phosphatized clasts they studied was a result of the Fe oxides, glauconite and of the high francolite content. In these nodules besides calcite, only CFA was detected and there were no traces of either glauconite or Fe oxides, probably because these phases were below the detection limit of powder diffraction method. The refinement of CFA lattice constants on 20 reflections gave the following parameters: $a = b = 9.3218$ Å; $c = 6.9146$ Å; $Z = 2$; unit-cell volume $= 520.35$ Å^3. Considering that in CFA the unit-cell a dimension can decrease approximately from 9.37 Å to 9.32 Å, because of carbonate substitution for phosphate (Zapata and Roy, 2004), the calculated figure, 9.3218 Å, indicates the high level of CO_3^{2-} substitution for PO_4^{3-}. The high CO_3^{2-} content in CFA structure is confirmed measuring the 2θ distance between the (410) and (004) CFA peaks. The calculated CO_3^{2-} in the lattice varies from 6.20 to 7.57 using the equation of Gulbrandsen (1970) and from 7.95 to 10.45 using the one proposed by Schuffert *et al*. (1990). A content of 1.4 CO_3^{2-} moles per formula wt. is obtained when this value is plotted on Figure 4 of Zapata and Roy (2004). This result is logical considering that older (i.e. Palaeozoic) phosphatic rocks generally contain a limited amount of substituted carbonate, while younger (i.e. Mio-Pliocenic) ones permit higher levels of CO_3^{2-} substitution for PO_4^{3-} (McClellan and Van Kauwenbergh, 2004).

OPTICAL LIGHT MICROSCOPY

OLM observation revealed the presence of abundant benthonic and planktonic foraminifera and smaller amounts of echinoid plates and bryozoans well-cemented together by sparitic calcite. The fauna observed in thin sections is almost the same as that described by Carbone *et al*. (1987), i.e., *Miogypsina* sp., *Amphistegina* sp., *Globigerinoides trilobus*, *Globigerinoides siakensis* and *Praeorbulina glomerosa*, as
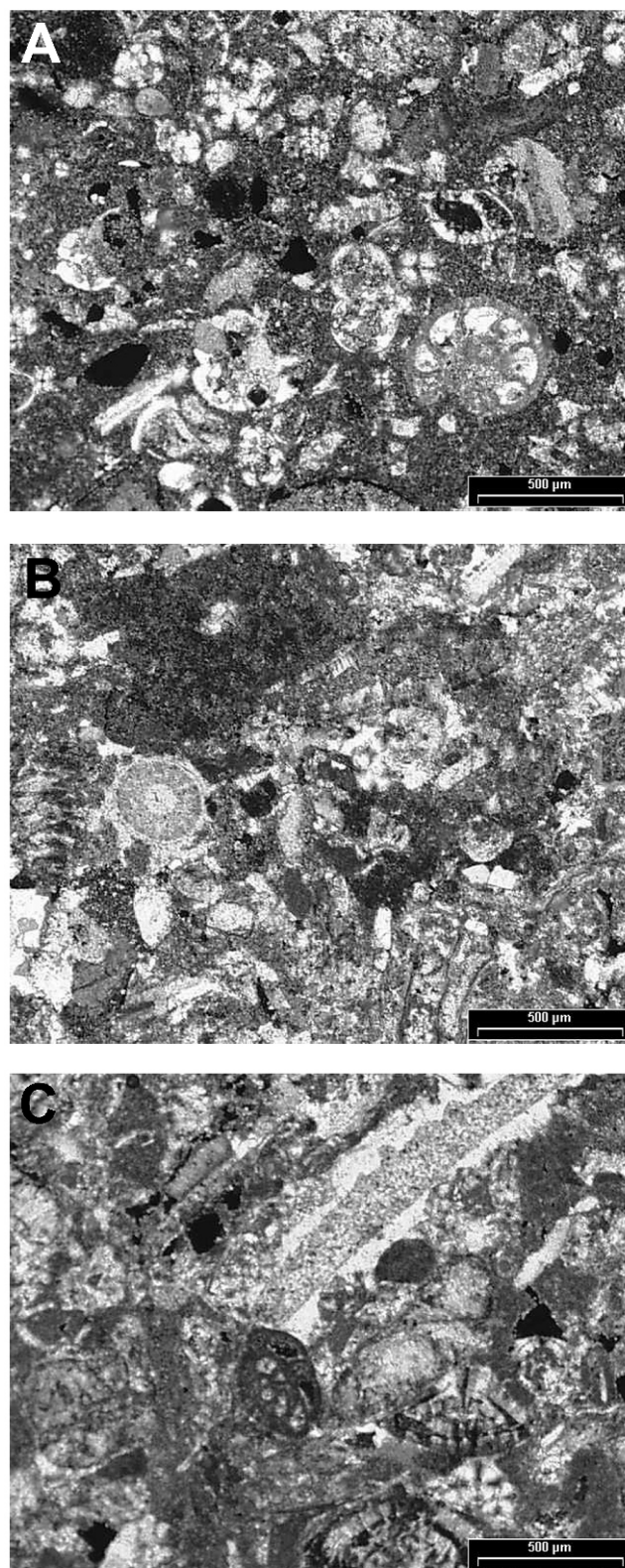

Fig. 4. OLM photographs of phosphorite nodules where micro-organisms well-cemented together by sparitic calcite can be observed (crossed nicols)

A — BR nodule with abundant benthic foraminifers; **B** — IR nodule with a sea urchin spine section and fragments of lamellibranches; **C** — DL nodule with various nummulites

well echinoid plates and coralline algae, indicating that these phosphates are of the Late Burdigalian age. Because of their submicroscopic dimensions, it was not possible to identify any CFA crystals with this technique. We could only identify a brownish micritic matrix which can suggest the presence of glauconite and/or Fe oxides (Fig. 4A, B and C). Intraparticle and interparticle porosity is very limited (~10%) and is generally observed inside hollow parts of bioclasts or between fragments within the matrix where secondary calcite has not totally filled the empty spaces.

FIELD EMISSION SCANNING ELECTRON MICROSCOPY

Secondary electron microphotographs show irregular surfaces that were mainly composed of micrometer calcite crystals. Hexagonal crystallites were identified as CFAs because EDX microanalysis confirmed the presence of Ca and P (Fig. 5A). The aforementioned crystals were ~600 nm in diameter and showed reduced growth along their c axis. The $\{0001\}_{CFA}$ and the $\{10\bar{1}0\}_{CFA}$ forms could be seen. The short c axis in CFAs has been attributed by Sánchez Navas and Martín Algarra (2001) to coalescence or coarsening mechanisms of earlier crystals that were longer and thinner and of amorphous phosphates. The short c axis would also seem to be a result of the high carbonate substitution which limits the size of the CFAs and makes them more equiaxial in shape (Nathan, 1984). At low magnifications the general appearance of these crystals suggests the presence of euhedral shapes (Fig. 5A), but when magnified they are clearly subhedral (Fig. 5B). In fact, all the crystals show imperfections. In some cases the centre of the crystal has not developed in the same way as the outer parts producing a hollow, skeletal shape. Similar shapes have been observed in phosphates by other authors and have been interpreted as the result of microbial activity which favours accretion mechanisms (Lucas and Prévôt, 1984; Soudry, 1994, 2000; Krajewski, 2000), even if there is no clear evidence that cellular bodies are necessary for the formation of CFAs (Krajewski et al., 1994). The absence of euhedral CFAs is common in many sedimentary phosphate deposits and they can also form directly from supersatured pore solutions. In most of the crystals, it is clear that the surface of the $\{0001\}_{CFA}$ face is not flat and is in fact slightly oval-shaped, which could suggest that pre-existing micro-organisms (i.e. bacteria) have been coated by francolite crystals (Fig. 5B and D). The crystals are randomly positioned with no preferential orientation and it is clearly possible to observe a porous space between them (Fig. 5A). The CFAs accumulate in confined microspaces such as pores, fissures or for example inside microborings (Fig. 5E and F). Figures 5G and H confirm these results as the CFAs do not replace skeletal material and appear, instead, in more sheltered areas nearby.

Figure 6A shows a BSE image of the phosphatic nodules. The union among grains is almost complete, porosity seems to be very low and pore interconnection is limited. Fragments of various microfossils are easily recognizable and subangular quartz grains can also be detected. They are minute (just a few micrometers) and could not therefore be seen with OLM. The spatial distribution of Ca, P and F was determined with the use of EDS by elemental mapping. In a map showing the distribution of Ca it was impossible to distinguish the bioclasts from the matrix because of the high concentration of Ca in the entire nodule; only isolated black areas, those with irregular-shaped pores, could be seen (Fig. 6B). P (Fig. 6C) and F content (Fig. 6D) were rather low compared to Ca and were distributed almost entirely in the matrix rather than in the shells of bioclasts and confirm the previous observations (Fig. 5G and H). However, it was impossible to see a more concentrated distribution of F and P (in the confined microspaces where CFAs crystallize, Fig. 5) because the magnification of SE and BSE images is different.

DISCUSSION

Phosphatic limestones outcrops are associated with the establishment of hardground conditions during the early Miocene period (Carbone et al., 1987). This work complemented and partially modified the interpretations of the previous authors by proposing that the crystallization of CFA began in the Ragusa Formation after an initial period of lithification of the sea-floor (carbonate cementation) and glauconite replacement in pore sediment. During this time, the hardground surface was characterized by an accumulation of bioclasts (benthonic and planktonic communities).

Phosphogenesis, which started within the pore-space of sediment, could have been the result of a bacterially-mediated precipitation of minute non-oriented ovoidal phosphate particles and it is presumable that bacteria were involved at the beginning of CFAs formation. The phosphate cementation followed the carbonate cementation filling up the pore-space in nodules (see the low porosity in Fig. 6). The lack of euhedral CFA crystals in the studied nodules cannot be considered a direct proof of bacterial phosphatization of sediment and inorganic precipitation of fluorapatite has been demonstrated in the laboratory (Van Cappellen and Berner, 1991). However, a supersaturation of this phase in the solution is required and it is known that the average concentration of P in seawater is only 0.09 mgL^{-1} (Ehrlich, 2002). Even if direct precipitation occurs, kinetic growth is very slow and the fluorapatite precipitation

Fig. 5. FESEM microphotographs of phosphatic nodules

A — general view of CFA crystals in BR nodules, notice that the crystals are almost of the same size; **B** — magnification of a portion of the previous figure (the area inside the white rectangle) in which can be seen the imperfections on the faces of the CFA crystals, the microanalysis of these crystals can be seen in the inset; **C** — formation of skeletal CFA crystals in a DL nodule; **D** — development of a rounded shape in $\{0001\}_{CFA}$ faces; **E** — elongated tubes partially empty composed of CFA crystals in RI nodules; **F** — detailed image of the previous photograph (the area inside the white rectangle) in which hexagonal CFA crystals can be recognized, the added spectrum shows the composition of these crystals; **G** — *dascyladal* alga composed of calcite (see the microanalysis); **H** — detailed image of the previous figure in which CFA crystals can be seen (white arrow), notice how these crystals develop only in the protected area of the matrix, not in the shell of the alga
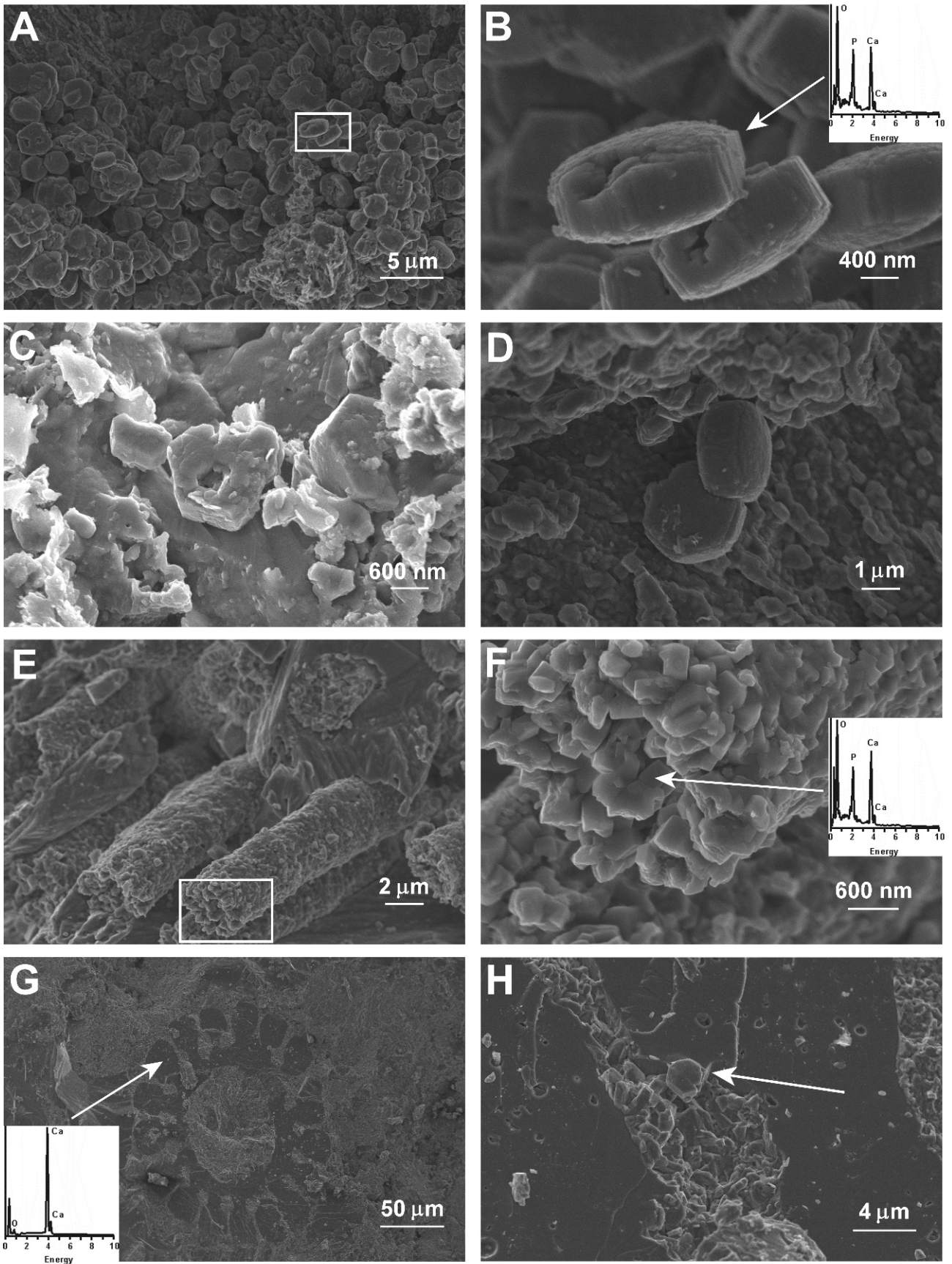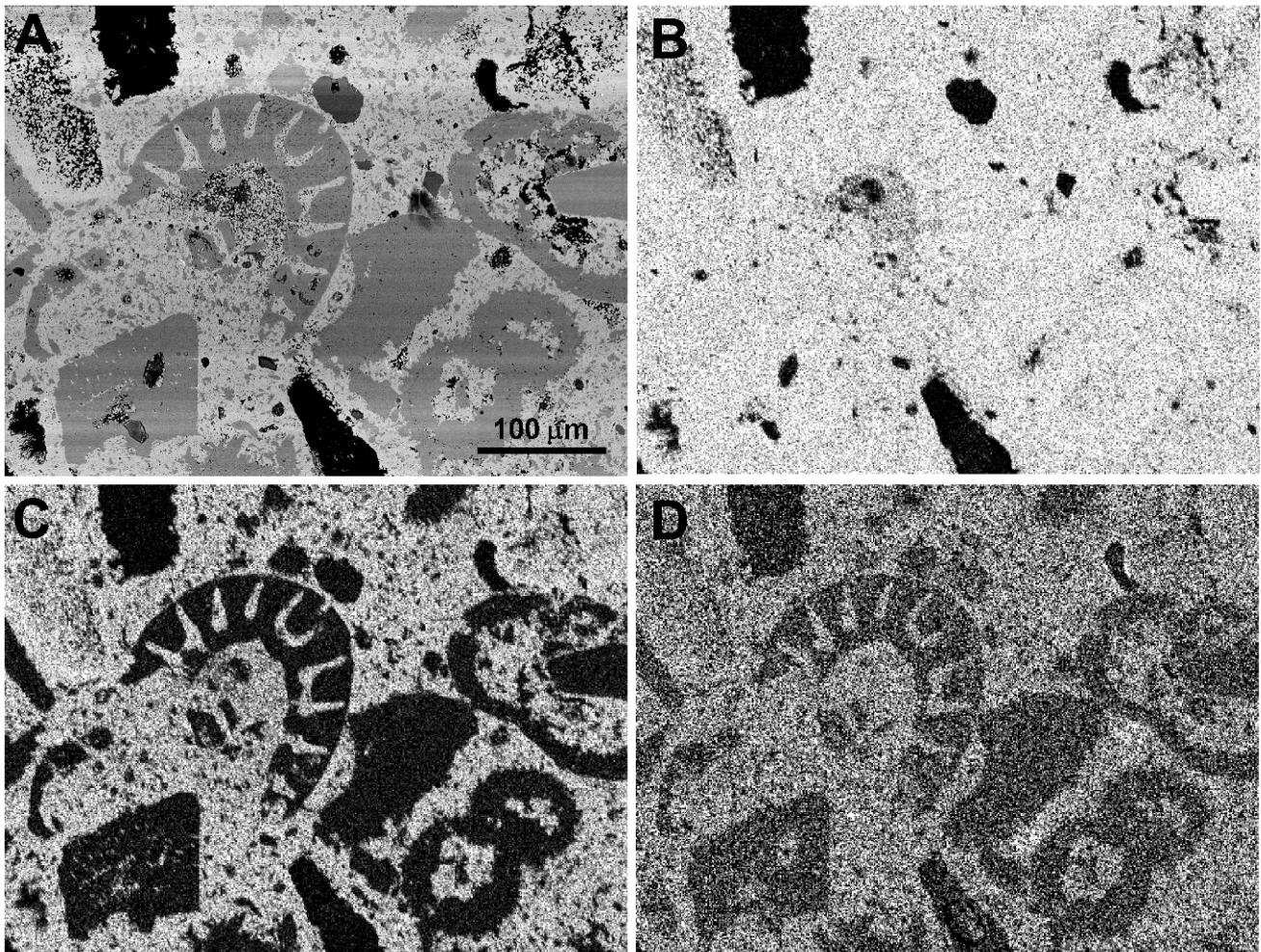
Fig. 6. BSE and X-ray images of a phosphatic nodule from the BR site

A — general view of the sample (BSE image), black areas correspond to pores and dark grey areas to small quartz grains; **B**–**D** — X-ray images of Ca, P and F, respectively, note the numerous nonphosphatized bioclastic fragments

rates are low (Krajewski *et al.*, 1994). Finally, a marked acceleration of current velocity within the sea-floor sediment was the responsible for the emergence of phosphatized nodules above the hardground (Carbone *et al.*, 1987).

Hence, bacteria could have provided the vehicle for phosphate mineralization due to the following considerations:

1. It was observed that the crystallization of CFA did not occur in microfossils shells. It usually develops in confined spaces inside the matrix (cavities, perforations, *etc.*) where organic matter may be easily accumulated. In these microenvironments microbial activity causes the production and breakdown of organic matter, the release of inorganic compounds and metabolic products, and it provides sites for the nucleation and growth of solid phases. The walls of bacterial cells are chemically reactive which facilitates the nucleation and growth of mineral phases (Ferris, 1997).

2. FESEM images highlight the absence of a preferred orientation of CFA crystals as well as the high porosity of these microenvironments where microbes could have been developed.

In these areas, which are supersaturated in P, soluble phosphate, liberated by bacteria, reacted with calcium ions forming insoluble calcium phosphate compounds (Ehrlich, 2002).

3. Notice how all the CFA crystallites are the same size (~1 μm). If bacteria promoted phosphogenesis, it would be reasonable to assume that CFAs would have equal dimensions. They allow the francolite to crystallize but, at the same time, their cells create a limit to the expansion of the crystallites.

4. All CFA crystals show some defects such as incomplete face growth, skeletal morphologies development and rounding of $\{0001\}_{CFA}$ faces. It seems that in the water-sediment surface there was a high phosphate supersaturation as a result of microbial proliferation and a rapid precipitation of CFAs in an environment full of impurities that causes such imperfections to occur (Krajewski, 2000). The major argument in favour of bacterial action in phosphogenesis should be the presence of abundant bacteria-like particles (Fountain and McClellan, 2000). The non-appearance of bacterial morphologies may be related to the fact that bacterial bodies were too delicate and ephemeral

to survive the diagenetic processes (Baturin, 2000). Cellular bodies are not necessaries for the formation of CFA, but it is known that their abundance leads to the common deposition of apatite (Krajewski *et al.*, 1994).

According to Ruttenberg and Berner (1993) and Schenau *et al.* (2000), it is possible to state that disseminated CFA crystals acted as a sedimentary sink for removal of the reactive phosphorus and fluorine in the sea so favouring the development of phosphatic nodules. High carbonate substitution for phosphate occurred during this time, as indicated by the low unit-cell *a* value. The phosphatised layers we studied were noticeably thin. This is because the precipitation of phosphates is generally restricted to the uppermost part of the sediment, and the increase of carbonate alkalinity in pore water below a depth of a few centimetres precludes further development of phosphatic minerals (Glenn and Arthur, 1988; Schenau *et al.*, 2000).

CONCLUSIONS

The formation of francolite (carbonate-fluorapatite) was investigated in south-east Sicilian phosphatic limestones. Such deposits were formed during long periods of hardground conditions. Phosphogenesis was mainly due to francolite precipita-tion within the pores sediment forming francolite crystals almost all of which measured ~1 μm in diameter. These crystals, of irregular morphology, precipitated in microenvironments supersaturated in P which probably had been produced by bacteria. Francolite crystallization only affected the matrix of the phosphatic nodules and did not affect the carbonate shells of benthic and planktonic foraminifera. It occurred in confined spaces where organic matter tended to accumulate. The reduced growth of these crystals along the *c* axis suggests two hypotheses: 1) they represent a second stage of recrystallization of earlier, thinner, more elongated crystals or 2) a high CO_3^{2-} substitution for PO_4^{3-} favoured the development of tabular-shaped crystals. In fact, the low value of the unit-cell *a* of francolite crystals indicates that they were subjected to high rates of carbonate for phosphate substitution, which normally occurs in young sedimentary phosphatic deposits.

REFERENCES

BATURIN G. N. (1971) — Formation of phosphate sediments and water dynamics. Oceanology, **11**: 372–376.

BATURIN G. N. (2000) — Formation and evolution of phosphorite grains and nodules on the Namibian shelf, from recent to Pleistocene. Marine Authigenesis, **66**: 185–199.

BIRCH G. F. (1979) — Phosphatic rocks on the western margin of South Africa. J. Sediment. Petrol., **49**: 93–110.

BOMMARITO S. and LA ROSA N. (1962) — Ricerche sulla estensione dell'orizzonte fosfatifero nella regione Iblea. Rivista Mineraria Siciliana, **13**: 1–7.

CARBONE S., GRASSO M., LENTINI F. and PEDLEY H. M. (1987) — The distribution and paleoenvironment of early Miocene phosphorites of Southeast Sicily and their relationships with the Maltese phosphorites. Paleogeogr. Paleoclimat. Paleoecol., **58**: 35–53.

CHEN D. F., DONG W. Q., ZHU B. Q. and CHEN X. P. (2004) — Pb-Pb ages of Neoproterozoic Doushantuo phosphorites in South China: constraints on early metazoan evolution and glaciation events. Precambrian Res., **132**: 123–132.

CHUNG F. H. (1974) — Quantitative interpretation of X-ray diffraction patterns. I. Matrix flushing method of quantitative multicomponent analysis. J. Appl. Crystallography, **7**: 519–525.

CORTESE E. (1929) — Fosfati naturali e loro utilizzazione. La Miniera Italiana, **16**: 116.

DE STEFANI C. (1912) — Noduli fosfatici nei dintorni di Siracusa. Atti della Soc. Toscana di Sc. Nat., P.V., 20.

DI GRANDE A., LO GIUDICE A. and BATTAGLIA M. (1978) — Dati geo-mineralogici preliminari sui livelli miocenici a fosfati di Scicli-Donnalucata (Sicilia SE). Boll. Soc. Geol. Italiana, **97**: 383–390.

EHRLICH H. L. (2002) — Geomicrobiology. Marcel Dekker, Inc., New York.

FERRIS F. G. (1997) — Formation of authigenic minerals by bacteria. In: Biological-Mineralogical Interactions (eds. J. M. McIntosh and L. A. Groat). Mineral. Ass. Canada, Short Course Ser., **25**: 187–208.

FOUNTAIN K. B. and McCLELLAN G. H. (2000) — Mineralogical and geochemical evidence for the origin of phosphorite nodules on the upper west Florida slope. Marine Authigenesis, **66**: 201–220.

FROELICH P. N., ARTHUR M. A., BURNETT W. C., DEAKIN M., HENSLEY V., JAHNKE R., KAUL L., KIM K. H., ROE K., SOUTAR A. and VATHAKANON C. (1988) — Early diagenesis of organic matter in Peru continental margin sediments: phosphorite precipitation. Marine Geol., **80**: 309–343.

GLENN C. R. and ARTHUR M. A. (1988) — Petrology and major element geochemistry of Peru margin phosphorites and associated diagenetic minerals: Authigenesis in modern organic-rich sediments. Marine Geol., **80**: 231–267.

GOVINDARAJU K. (1989) — Compilation of working values and samples description for 272 geostandards. Geostandards Newsletter, Spec. Iss., **13**: 1–113.

GRASSO M. (1997) — Geological map of the south-central sector of Iblean plateau (Province of Ragusa, SE Sicily), scale 1:50 000.

GULBRANDSEN R. A. (1970) — Relation of carbon dioxide content of apatite of the Phosphoria Formation to regional facies. US Geol. Surv. Prof. Pap., **700B**: B9–B13.

GUNNARS A., BLOMQVIST S. and MARTINSSON C. (2004) — Inorganic formation of apatite in brackish seawater from the Baltic Sea: an experimental approach. Marine Chemistry, **91**: 15–26.

ILYIN A. (1997) — Mid-Cretaceous phosphate platforms of the Russian Craton. Sediment. Geol., **113**: 125–135.

JARVIS I. (1992) — Sedimentology, geochemistry and origin of phosphatic chalks: the Upper Cretaceous deposits of NW Europe. Sedimentology, **39**: 55–97.

KIM D., SCHUFFERT J. D. and KASTNER M. (1999) — Francolite authigenesis in California continental slope sediments and its implications for the marine P cycle. Geochim. Cosmochim. Acta, **63**: 3477–3485.

KIM K. H. and BURNETT W. C. (1988) — Accumulation and biological mixing of Peru Margin sediments. Marine Geol., **80**: 181–194.

KNIGHT R. (1999) — Phosphates and phosphogenesis in the Gault Clay (Albian) of the Anglo-Paris Basin. Cretaceous Res., **20**: 507–521.

KRAJEWSKI K. P. (2000) — Diagenetic recrystallization and neoformation of apatite in the Triassic phosphogenic facies in Svalbard. Stud. Geol. Pol., **116**: 111–137.

KRAJEWSKI K. P., VAN CAPPELLEN P., TRICHET J., KUHN O., LUCAS J., MARTÍN ALGARRA A., PRÉVÔT L., TEWARI V. C., GASPAR L., KNIGHT R. I. and LAMBOY M. (1994) — Biological processes and apatite formation in sedimentary environments. Eclogae Geol. Helvetiae, **87**: 701–745.

LEGEROS R. Z. (1965) — Effect of carbonate on the lattice parameters of apatite. Nature, **24**: 403–404.

LUCAS J. and PRÉVÔT L. (1984) — SynthPse de l'apatite par voie bactérienne B partir de matiPre organique phosphatée et de divers car-bonates de calcium dans des eaux douce et marine naturelles. Chem. Geol., **42**: 101–118.

MARSHALL G. and RUFFELL A. (2004) — Authigenic phosphate nod-ules (Late Cretaceous, Northern Ireland) as a condensed succession microarchives. Cretaceous Res., **25**: 439–452.

MARTÍN ALGARRA A. and SÁNCHEZ NAVAS A. (1995) — Phosphate stromatolites from condensed chephalopod limestones, Upper Jurassic, Southern Spain. Sedimentology, **42**: 893–919.

MARTÍN ALGARRA A. and SÁNCHEZ NAVAS A. (2000) — Bacterially mediated authigenesis in Mesozoic stromatolites from condensed pe-lagic sediments (Betic Cordillera, Southern Spain). In: Marine Authigenesis: from global to microbial (eds. C. R. Glenn, L. Prévôt. and J. Lucas). SEPM Spec. Publ., **66**: 499–525.

MARTÍN J. D. (2004) — Using XPowder: A software package for Powder X-Ray diffraction analysis. www.xpowder.com, Legal Deposit GR 1001/04. ISBN 84-609-1497-6. 105 p. Spain.

MATTHEWS A. and NATHAN Y. (1977) — The decarbonation of carbon-ate-fluorapatite (francolite). Am. Mineralogist, **62**: 565–573.

McCLELLAN G. H. and VAN KAUWENBERGH S. J. (2004) — Charac-terization of phosphate rocks. In: Use of phosphate rocks for sustain-able agriculture (eds. F. Zapata and R. N. Roy). FAO Fertilizers and Plant Nutrition Bull., **13**: 17–26.

NATHAN Y. (1984) — The mineralogy and geochemistry of phosphorites. In: Phosphate Minerals (eds. J. O. Nriagu and P. B. Moore): 275–291. Springer-Verlag. New York.

PEDLEY M. and BENNETT S. M. (1985) — Phosphorites, hardgrounds and syndepositional subsidence structures: a paleoenvironmental model from the Miocene of the Maltese Islands. Sediment. Geol., **45**: 1–34.

PURNACHANDRA RAO V., MOHAN RAO K. and RAJU D. S. N. (2000) — Quaternary phosphorites from the continental margin off Chennai, southeast India: analogs of ancient phosphate stromatolites. J. Sediment. Res., **70**: 1197–1209.

RAGUSA E. (1902) — Ritrovamento di fosfati a Modica. Boll. Accad. Gioenia Sc. Natur. Catania, **71**: 12–21.

REIMERS C. E., KASTNER M. and GARRISON R. E. (1990) — The role of bacterial mats in phosphate mineralization with particular reference to the Monterrey Formation In: Phosphorite Deposit of the World (eds. W. C. Burnett and S. R. Riggs). Cambridge Univ. Press, **3**: 300–311.

RUTTENBERG K. C. and BERNER R. A. (1993) — Authigenic apatite formation and burial in sediments from non-upwelling, continental margin environments. Geochim. Cosmochim. Acta, **57**: 991–1007.

SÁNCHEZ NAVAS A. and MARTÍN ALGARRA A. (2001) — Genesis of apatite in phosphate stromatolites. European J. Mineral., **13**: 361–376.

SCHENAU S. J., SLOMP C. P. and DE LANGE G. J. (2000) — Phosphogenesis and active phosphorite formation in sediments from the Arabian Sea oxygen minimum zone. Marine Geol., **169**: 1–20.

SCHUFFERT J. D., JAHNKE R. A., KASTNER M., LEATHER J., STURZ A. and WING M. R. (1994) — Rates of formation of modern phosphorite off western Mexico. Geochim. Cosmochim. Acta, **58**: 5001–5010.

SCHUFFERT J. D., KASTNER M., EMANUELE G. and JAHNKE R. A. (1990) — Carbonate-ion substitution in francolite: a new equation. Geochim. Cosmochim. Acta, **54**: 2323–2328.

SCHWENNICKE T., SIEGMUND H. and JEHL C. (2000) — Marine phosphogenesis in shallow-water environments: Cambrian, Tertiary, and recent examples. Marine Authigenesis, **66**: 481–498.

SLANSKY M. (1979) — Proposal for the nomenclature and classification of the sedimentary phosphate rocks. In: Proterozoic-Cambrian Phosphorites (eds. J. Cooke and J. H. Shergold): 60–63. Canberra.

SCOTT V. D. and LOVE G. (1983) — Quantitative electronprobe microanalysis. John Wiley and Sons, New York.

SOUDRY D. (1993) — Internal structure and growth of an intraformational concretional phosphorite from an early Tertiary starved-sediment sequence: Árava Valley, Southern Israel. Kaupia, Darmstädter Beiträge zur Naturgeschichte, **2**: 67–76.

SOUDRY D. (1994) — Bottom-dwelling microphytes and phosphate sedi-ment accretion: the case of the Campanian phosphorites, Negev, South-ern Israel. Kaupia, Darmstädter Beiträge zur Naturgeschichte, **4**: 61–70.

SOUDRY D. (2000) — Microbial phosphate sediments. In: Microbial Sed-iments (eds. R. E. Riding and S. M. Awramik): 127–136. Springer-Verlag.

SOUDRY D. and NATHAN Y. (2000) — Microbial infestation: a pathway of fluorite enrichment in bone apatite fragments (Negev phosphorites, Israel). Sediment. Geol., **132**: 171–176.

TEDESCO C. (1966) — Ricerche sulle mineralizzazioni fosfatiche della Sicilia orientale ed esame comparativo dei metodi di prospezione. Rivista Mineraria Siciliana, **97–99**: 3–17.

VAN CAPPELLEN P. and BERNER R. A. (1991) — Fluorapatite crystal growth from modified seawater solutions. Geochim. Cosmochim. Acta, **55**: 1219–1234.

ZAPATA F. and ROY R. N. (2004) — Introduction. In: Use of Phosphate Rocks for Sustainable Agriculture (eds. F. Zapata and R. N. Roy). FAO Fertilizers and Plant Nutrition Bull., **13**: 1–9.

ZHANG G., GERMAINE J. T., MARTIN R. T. and WHITTLE A. J. (2003) — A simple sample-mounting method for random powder X-ray dif-fraction. Clays and Clay Minerals, **51**: 218–225.